Low Cost High Efficiency Photovoltaics Using Semiconductor Nanocrystals

Cooperative Research and Development Final Report

CRADA Number: CRD-15-00598

NREL Technical Contact: Matthew C. Beard

NREL is a national laboratory of the U.S. Department of Energy
Office of Energy Efficiency & Renewable Energy
Operated by the Alliance for Sustainable Energy, LLC

This report is available at no cost from the National Renewable Energy Laboratory (NREL) at www.nrel.gov/publications.

Contract No. DE-AC36-08GO28308

Technical Report
NREL/TP-5900-81994
January 2022

Low Cost High Efficiency Photovoltaics Using Semiconductor Nanocrystals

Cooperative Research and Development Final Report

CRADA Number: CRD-15-00598

NREL Technical Contact: Matthew C. Beard

Suggested Citation
Beard, Matthew C. 2022. *Low Cost High Efficiency Photovoltaics Using Semiconductor Nanocrystals: Cooperative Research and Development Final Report, CRADA Number CRD-15-00598.* Golden, CO: National Renewable Energy Laboratory. NREL/TP-5900-81994. https://www.nrel.gov/docs/fy22osti/81994.pdf.

NREL is a national laboratory of the U.S. Department of Energy
Office of Energy Efficiency & Renewable Energy
Operated by the Alliance for Sustainable Energy, LLC

This report is available at no cost from the National Renewable Energy Laboratory (NREL) at www.nrel.gov/publications.

Contract No. DE-AC36-08GO28308

Technical Report
NREL/TP-5900-81994
January 2022

National Renewable Energy Laboratory
15013 Denver West Parkway
Golden, CO 80401
303-275-3000 • www.nrel.gov

NOTICE

This work was authored by the National Renewable Energy Laboratory, operated by Alliance for Sustainable Energy, LLC, for the U.S. Department of Energy (DOE) under Contract No. DE-AC36-08GO28308. Funding provided by the U.S. Department of Energy, Office of Science, Basic Energy Sciences. The views expressed herein do not necessarily represent the views of the DOE or the U.S. Government.

Cover Photos by Dennis Schroeder: (clockwise, left to right) NREL 51934, NREL 45897, NREL 42160, NREL 45891, NREL 48097, NREL 46526.

NREL prints on paper that contains recycled content.

Cooperative Research and Development Final Report

Report Date: January 25, 2022

In accordance with requirements set forth in the terms of the CRADA agreement, this document is the CRADA final report, including a list of subject inventions, to be forwarded to the DOE Office of Scientific and Technical Information as part of the commitment to the public to demonstrate results of federally funded research.

Parties to the Agreement: Korea Institute of Machinery and Materials (KIMM)

CRADA Number: CRD-15-00598

CRADA Title: Low Cost High Efficiency Photovoltaics Using Semiconductor Nanocrystals

Responsible Technical Contact at Alliance/National Renewable Energy Laboratory (NREL):

Matthew C. Beard | matt.beard@nrel.gov

Name and Email Address of POC at Company:

Sohee Jeong | S.jeong@kimm.re.kr

Sponsoring DOE Program Office(s):

Office of Science, Basic Energy Sciences (BES) Program

Joint Work Statement Funding Table showing DOE commitment:

No NREL Shared Resources

Estimated Costs	NREL Shared Resources a/k/a Government In-Kind
Year 1	$.00
TOTALS	$.00

Executive Summary of CRADA Work:

Collaboration will occur between NREL and KIMM in the area of semiconductor nanocrystals for use in advanced solar photon energy conversion strategies. The project takes advantage of the unique capabilities and expertise regarding the incorporation of quantum dots (QD) into solar energy technologies that are available at NREL within the BES-funded programs. KIMM has unique expertise in the synthesis of new types of nanocrystals as well as advanced processes for solution processing.

Summary of Research Results:

Task One

Objective: Determine new candidate QDs with high multiple-exciton generation (MEG) efficiencies.

In collaboration with KIMM, NREL will measure the carrier dynamics of candidate QD materials to determine their suitability and determine the appropriate QDs that have sufficient MEG characteristics for solar cell incorporation. The candidate materials include the exploration of ternary low bandgap semiconductors.

1.1 Exploration of ternary low bandgap semiconductors.

We successfully synthesized nanocrystals of $AgSbS_2$, and $AgSbSe_2$ a I-V-VI semiconductor (see Scheme 1 for general approach). The synthesis of $AgSbTe_2$ was not successful. The stability of $AgSbSe_2$ was not sufficient to fabricate NC based solar cells so we focused our initial attention on $AgSbS_2$ nanocrystals.

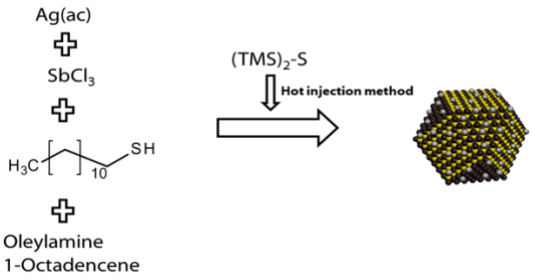

Scheme 1. Illustration of simple synthesis process to $AgSbS_2$ QDs

In our system, the colloidal $AgSbS_2$ QDs were synthesized by reacting silver acetate (Ag(ac)), antimony chloride ($SbCl_3$) with bis (trimethylsilyl) sulfide ($(TMS)_2$-S) in 1-octadecene (ODE) solvent. Oleylamine (OLA) and 1-dodecanethiol (DDT) were used as stabilizers. Especially, the DDT amount was elaborately controlled because it plays a significant role in synthesizing size tuned $AgSbS_2$ QDs. Silver acetate and antimony chloride was added to ODE solution which has OLA and DDT, then heated to 105 °C and maintained while stirring under vacuum for 1 hour. Figure 1 shows TEM of the NCs for different sizes as well as the XRD showing the α-miargyrite phase. The optical data suggest that these particles have an indirect bandgap. The $AgSbSe_2$ have a much lower (IR) optical absorption onset (not shown). The lower bandgap is more attractive for solar PV applications. However, as proof-of-principle we demonstrated that solar cells can be fabricated from the $AgSbS_2$ nanocrystals (see task 2 below).

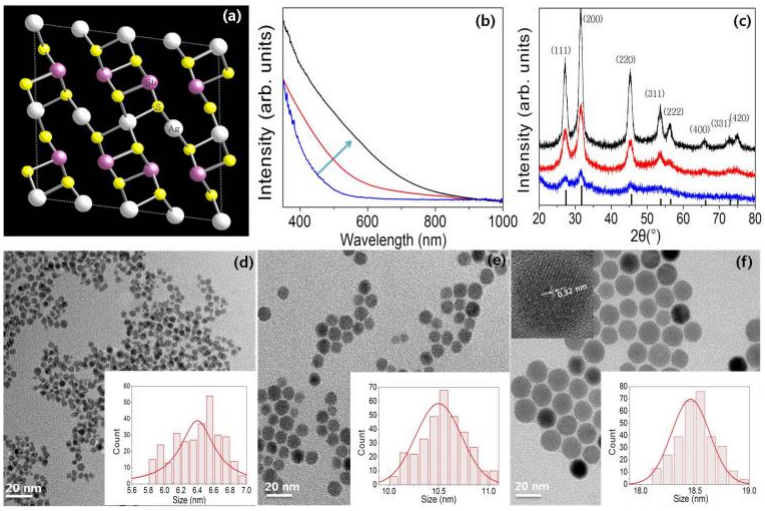

Figure 1(a) Crystal structure (α-miargyrite) of $AgSbS_2$ QDs, (b) Optical absorption spectra for the three samples with varying DDT concentration from 0.90 mmol (blue line) and 0.45 mmol (red line), with one sample was synthesized without DDT (black line) (c) XRD patterns (d-f) TEM, HR-TEM (inset) images of various sized $AgSbS_2$ NCs. Corresponding of the particle size distribution histograms and Gaussian fit distribution (right inset in figure d-f)

1.2 Exploration of $AbSbTe_2$

We attempted the synthesis of $AbSbTe_2$ but the resulting samples were not of the correct stoichiometry and the were not NCs. Thus, the synthesis failed and we focused on CdS/PbS Janus NCs discussed in section 1.3

During the course of the project we identified a new quantum confined system that could be of value to the goals of the project.

PbS/CdS heterostructures

PbS/CdS heterostructure NCs were fabricated following our previous method developed at NREL in which partially cation exchanged CdS QDs result in PbS/CdS Janus-like particles. It was found that varying the reaction temperature, time, and the Pb-to-Cd precursor ratios allowed for control over the extent of exchange of the original CdS QD. Figure 2A shows an example of the absorbance spectra of the precursor CdS QDs and the product PbS/CdS heterostructures. The extent of exchange is estimated by the relative X-ray diffraction (XRD) peak intensities. Figure 2B shows an example XRD spectrum in which the extent of exchange is estimated to be ~50%. Figure 2C-D shows TEM images of precursor CdS QDs and the post-exchange PbS/CdS heterostructures, respectively, which are used to further characterize Janus-like NCs. Janus-like NCs are clearly visible by a lattice boundary, which can be further used to characterize the extent of exchange. Additionally, the PbS/CdS Janus-like NCs are seen to be approximately half the size (~5 nm) of the intial CdS QDs (~10 nm), which suggests that CdS NCs break up during exchange

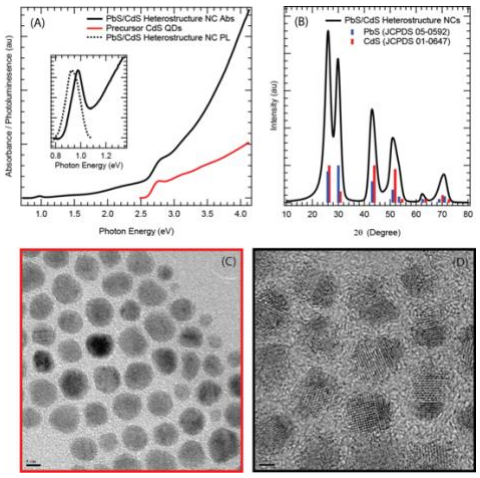

Figure 2. Characterization of synthetic QD precursor and heterostructure product (A) UV-Vis-NIR absorbance spectra of precursor CdS QDs (red) and PbS/CdS heterostructure NCs (black). Inset shows the expanded first exciton absorbance spectrum as well as the photoluminescence spectrum of the PbS/CdS heterostructure. (B) XRD pattern of the PbS/CdS heterostructure NCs. TEM images are shown of (C) initial CdS QDs used for cation exchange and (D) resulting PbS/CdS heterostructure NCs.

1.3 Test MEG of the newly developed NCs using TA spectroscopy

We focused our spectroscopic characterization on the PbS/CdS material system.

Our results show that these nanocrystals exhibit enhanced MEG over nanocrystals composed of only a single material, such as PbS and PbSe, as well as PbSe/CdSe core/shell QDs (Fig. 3). We attribute this MEG enhancement to a slowing of the hot exciton cooling rate, k_{cool}, and an increase in the MEG rate, k_{MEG}, due to increased exciton Coulombic coupling. The threshold energy has been reduced to 2Eg in these structures and then increases to about 1.2 e-h hole pairs per QD. There seems to be a second onset that occurs around 3 E_g which further increases the MEG performance. The performance of the Janus particles mirrors that of the core/shell particles but performs slightly better. We believe this is due to the anisotropic nature of the wavefunctions in both the core/shell structure as well as the Janus structures. The anisotropy is greater in the Janus particles leading to a higher Coloumbic interactions and a higher MEG performance. This result is published in ACS Nano, *ACS Nano*, 12, 10, 10084-10094, 2018.

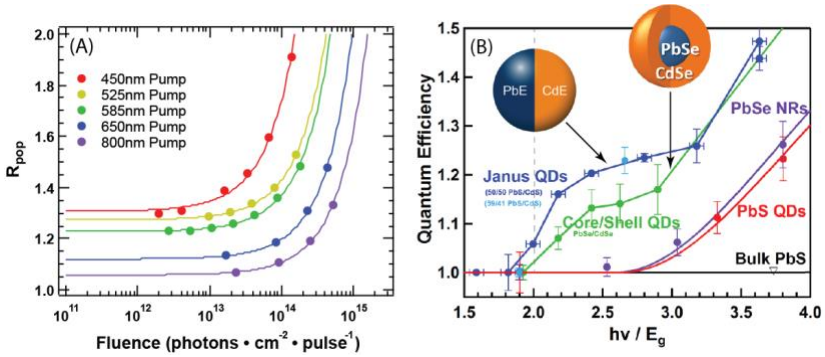

Figure 3. (A) Representative ratio of exciton population, R_{pop}, plotted versus the pump photon fluence for various pump wavelengths. (B) Photon-to-exciton quantum efficiencies versus bandgap normalized pump photon energy. Blue markers represent PbS/CdS heterostructure NCs and green markers represent PbSe/CdSe core/shell QDs measured at LANL. The purple, red, and black markers represent previously reported MEG measurements for PbSe nanorods, PbS quantum dots, and bulk PbS, respectively. The dashed gray line indicates the MEG energy conservation threshold for photon energies greater than 2x the NC bandgap.

Task 1.4 Exploration of Cd_3As_2 and Cd_sP_2

We synthesized Cd3As2 and Cd3P2 and tested their MEG efficiency. We did not find any enhanced MEG over that of pure phase PbS and PbSe QD samples. Therefore we decided to focus on a more interesting system namely atomically thin PbS nanocrystals.

Atomically Thin Metal Sulfides (ATMS) (PbS)

We developed a method to colloidally synthesize ATMS. The synthesis proceeds via a cation-exchange reaction starting from single and multi-layer Ag_2S and going to various metal sulfides. The synthesized ATMS retain their size and shape during the cation-exchange reaction and are either single-layer or a few-layer depending on the starting Ag_2S samples. They have lateral dimensions on the order of 5-10 nm and are colloidally stabilized by Z and L-type ligands. Here, we demonstrate the synthesis of single-layer and a few-layer ZnS, CdS, CoS_2, and PbS. We find that the optical properties of these ATMS are quite distinct from the platelet or quantum-dot versions of the same metal sulfides. Due to the unique nature of the ATMS and the enhanced spin-orbit coupling in the PbS ATMS we expect their photophysics to behave quite distinctly. We hypothesize that the MEG characteristics should be much larger and this is being currently tested. This result is published in JACS *JACS*, 141, 30, 12121-12127, 2019.

Task Two

Objective: Use candidate QD materials to plan and design suitable PV architectures.

2.1 Fabrication of solution PbSe deposited Solar Cells under ambient conditions.

PbSe QDs show a higher MEG than do PbS QDs. Yet most the QD solar cell fabrication has been done with PbS QDs partly because PbS is more stable in air than are PbSe QDs. Here, we developed a single step, cation-exchange reaction that produces air stable PbSe QDs from ZnSe QDs and PbX_2 (X=Cl, Br, or I) precursors. Since the resulting PbSe QDs are terminated with halide anions and contain residual Zn cations they are more stable in ambient conditions. Solar cells fabricated from these PbSe QDs obtained an overall best power conversion efficiency of 6.47% at one sun illumination. The solar cell performance without encapsulation remains unchanged for over 50 days in ambient conditions; and after 50 days, the NREL certification team certified the device at 5.9%. This result is published in ACS Nano, *ACS Nano*, 9, 8157-8164, 2015.

2.2 Fabrication of solution $AgSbS_2$ deposited Solar Cells

The $AgSbS_2$ QDs were deposited on top of the TiO_2 *via* spin coating at 2000 rpm from a 20 mg/mL hexane/dichlorobenzene solution. In order to promote adhesion of the $AgSbS_2$ QDs to the TiO_2 surface, the TiO_2 layer was treated with a 3 wt % EDT linker in ethanol solution. The cross-sectional SEM image (Fig. 4b) indicates that the $AgSbS_2$ QDs infiltrate to the mp-TiO_2 layer. The J-V curves in Fig. 2(c) indicate that the best results of the $AgSbS_2$ QD device showed a short circuit current density (J_{sc}) of 12.3 mA /cm^2, open circuit voltage (V_{oc}) of 0.49 V, fill factor (FF) 52 %, and an overall power conversion efficiency (η) of 3.13 % under AM 1.5 illumination. Figure 2(d) shows that the $AgSbS_2$ NCs hetero-junction photovoltaic cell exhibits > 30 % EQE across whole visible region and absorbs photons up to the 900 nm wavelength region. The integration of this EQE spectrum with the solar spectrum yields an integrated J_{sc} value of 11.9 mA/cm^2 in good agreement with the measured J_{sc}. A histogram of efficiency values (η) for 20 samples is presented in Fig. 4d inset. The EQE spectrum clearly indicates that this simple $AgSbS_2$ NC photovoltaic device can be applied to solar cells or photodetectors utilizing visible to near-infrared (NIR) light.

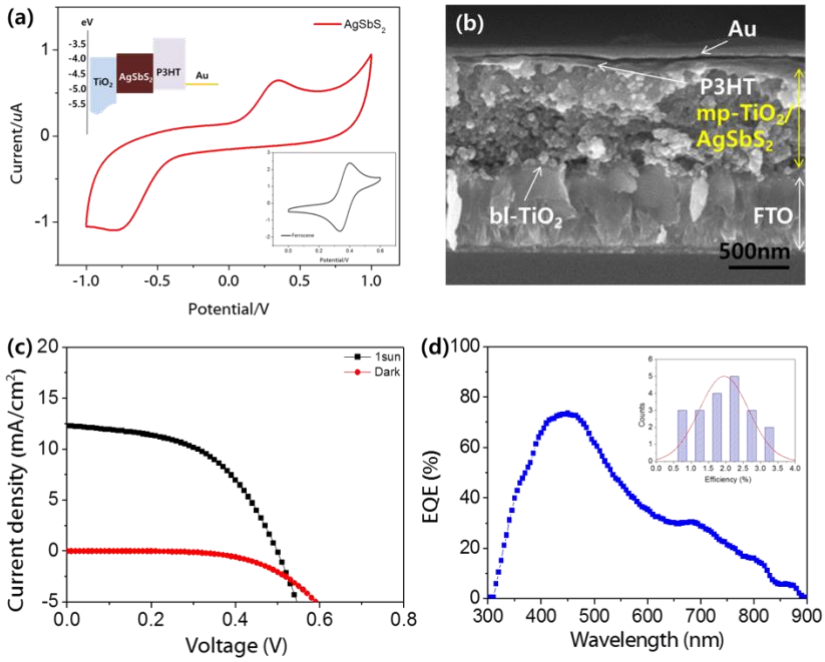

Figure 4 (a) the CV data of $AgSbS_2$ and energy band diagram (inset), (b) SEM cross-sectional image, (c) photocurrent density-voltage (J-V) curves, and (d) external quantum efficiency (EQE) spectrum of mesoscopic $AgSbS_2$ sensitized solar cell. Histogram of solar cell efficiencies for 20 samples (inset)

2.2 Fabrication of solution PbS/CdS deposited Solar Cells

Unlike PbSe/CdSe core/shell QDs, Janus-like NCs present the opportunity for incorporation as the active layer in photovoltaic devices. This is due to the fact that within Janus-like NCs, photogenerated charge carriers are delocalized with respect to the heterostructure and can therefore be extracted in solar cells. This is a significant advantage over PbSe/CdSe core/shell structures where photogenerated holes are localized to the QD core and become trapped. We constructed several solar cells by depositing Janus-like NCs on TiO_2-coated FTO/glass substrates. Films were cast using a layer-by-layer dipcoating method in which each layer was treated in a 1 mM solution of 1,2-ethanedithiol (EDT) in acetonitrile to displace oleate ligands. A MoO_x/Au top contact was then thermally evaporated. Top performing devices achieved nearly 3% efficiency with a 20.5 mA/cm^2 short-circuit current density and 307 mV open-circuit voltage (Figure 5). Additionally, the external quantum efficiency is seen to peak above 75% for Janus-like NCs with a 0.88 eV band gap.

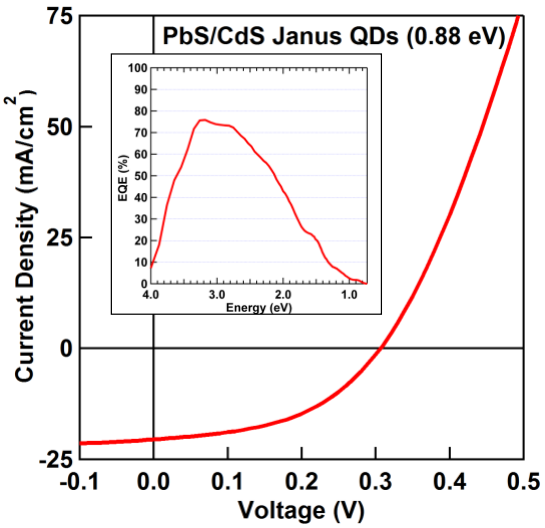

Figure 5. Current-voltage data for an EDT-treated Janus particle solar cell achieving nearly 3% efficiency. Insert shows external quantum efficiency (EQE) for the device.

2.3 Exploration of Solution processable tandem nanocrystal solar cells.

In addition to the enhanced MEG effect in semiconductor nanocrystals inexpensive solution deposited tandem devices can also yield a power conversion efficiency that exceeds the SQ-limit. We explored to the use of PbS QDs in a tandem configuration with CdTe. In the 2-terminal series connected tandem configuration, depending on the chosen top cell, there is a specific corresponding bottom cell E_g required to achieve optimal performance. However, as is shown in Fig. 6b if we enable the thickness of the top cell to vary, a controlled number of photons normally absorbed in the top cell could be transmitted to the bottom cell to aid in matching the current produced by each subcell since the overall current of the system is limited by the lowest producing subcell. Allowing the thickness of the top cell to vary enables a much wider range of E_g combinations that still achieve near-peak efficiency. Figure 6c, shows the analysis for a two-terminal, two-junction tandem solar cell with the top cell bandgap fixed (E_g = 1.5 eV) for CdTe. The ability to tune the thickness of the CdTe shows a widening of the range of bottom cells that could be paired with CdTe to still achieve high efficiencies. For example, a low bandgap absorber ranging between 0.68 and 1.16 eV could achieve a PCE above 40%. This ability to tailor the thickness of the CdTe is critical to enable a bottom cell with bandgap above 0.8 eV (the infinite thickness limit is shown as the dashed trace).

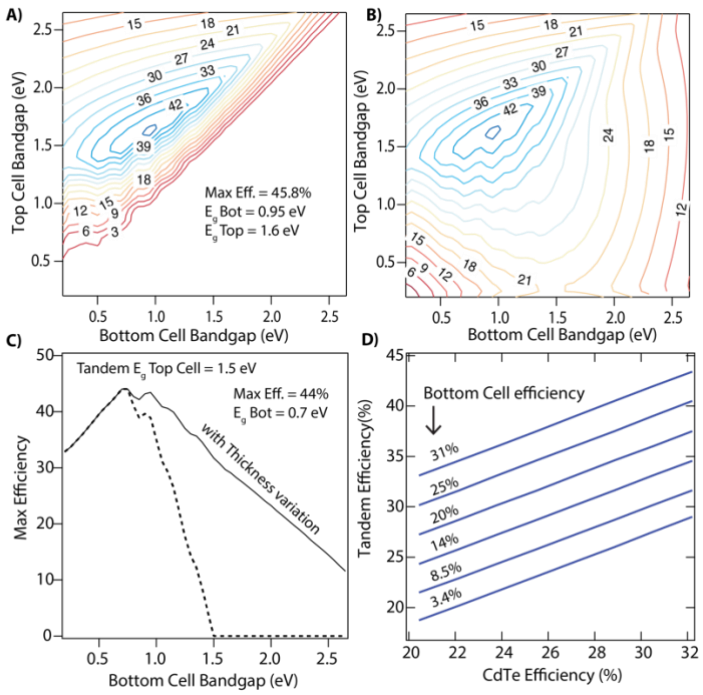

Figure 6. (a) Detailed balance efficiency limits for a dual-junction tandem solar cell assuming monolithic integration (i.e. two-terminal), AM1.5G spectrum, and that each cell absorbs all available photons with energy greater than the bandgap. (b) Same assumptions as in panel a) with the exception that the top cell thickness can be adjusted to permit some photons to be transmitted to the bottom cell. *Note: the thickness of the top cell for each optimized point in the contour may be different*. (c) Assuming the top cell has a bandgap of 1.5 eV (as does CdTe), the maximum efficiency of the tandem device is plotted as a function of the bottom cell bandgap under two conditions: infinite thickness approximation (dashed trace) and allowing the top cell thickness to vary (solid line). In both cases the most optimal condition yields a tandem cell with 44% efficiency with bottom cell bandgap of 0.7 eV. However, the solid trace shows near-optimal performance for a much wider range of bottom cell conditions. (d) Real world simulations of tandem cell efficiencies including non-radiative recombination losses. Lines show how the tandem cell efficiency would improve as a function of CdTe efficiency given a bottom cell efficiency with band gap of 0.95 eV.

Next, in our simulations we take into consideration that the present-day CdTe system does not operate at the radiative limit. We include non-radiative recombination through the external radiative efficiency (ERE). If the ERE is limited to 10^{-4}% to reflect present-day CdTe technologies, then the maximum efficiency attainable by a single junction CdTe cell (E_g = 1.5 eV) is 22% (as has been experimentally demonstrated). Pairing this quality of CdTe absorber with a 0.95 eV bottom cell that exhibits a single junction PCE of 14% (same ERE value as CdTe) could achieve a tandem cell efficiency of ~26%. We should note that in order to achieve higher efficiencies in these non-ideal cases where non-radiative recombination reduces the open circuit voltage the top cell must be thinned in order to utilize a bottom cell with a higher voltage but that is still current matched. Both CdTe efficiencies and low band gap efficiencies will improve over time as the technologies mature. We show how the tandem cell efficiency varies with the CdTe efficiency and bottom cell efficiency ($E_{g,Bottom}$ = 0.95 eV) in Fig. 6d. When the bottom cell has efficiency less than 9%, a tandem with CdTe of efficiency > 20% will not increase the overall efficiency. However, no matter how the efficiency of the CdTe sub-cell

improves over time a tandem cell with a bottom cell efficiency of 14% would add about 4% absolute (22% CdTe to 26% tandem, an 18% relative improvement) to the overall cell efficiency. If the bottom cell efficiency also improves then this number grows from 4% to ~ 12% absolute improvement (40% relative improvement), for the ideal case the single CdTe cell efficiency is 32% and the tandem cell efficiency would be 44%. PbS quantum dots (QDs) present a unique and attractive option for use in multi-junction solar energy conversion architectures due to their easily tunable bandgap (by varying the average QD size) across a wide range of energies. Furthermore, QD layers can be deposited in ambient conditions using low-cost, solution-processing methods. Low bandgap Pb-chalcogenide QDs and other materials also offer the advantage of producing multiple excitons per absorbed high-energy photon.

Task Three

Objective: Report and publish results

Based upon the work described in task 1 and 2 we contributed to the following 5 published manuscripts.

1. S. Kim, A.R. Marshall, E.M. Miller, D.M. Kroupa, J.M. Luther, S. Jeong, M.C. Beard, "Air Stable and Efficient PbSe Quantum Dots Solar Cells Based Upon Cation Exchange from ZnSe Quantum Dots", *ACS Nano*, 9, 8157-8164, **2015** doi: 10.1021/acsnano.5b02326

2. Choi, H., S. Kim, J.M. Luther, S.W. Kim, S. Dongwoon, M.C. Beard, S. Jeong, "Facet-Specific Ligand Interaction on Ternary $AgSbS_2$ Colloidal Quantum Dots: Enhanced Air-Stability via Thiolate Passivation", *Chem. Eur. J.23,1-8*, **2017,** doi:10.1002/chem.201703681

3. D. M. Kroupa, G. F. Pach, M. Vörös**,** F. Giberti, R. W. Crisp, B. D. Chernomordik, A. J. Nozik, J. C. Johnson, V. I. Klimov, G. Galli, and M. C. Beard, "Enhanced Multiple Exciton Generation in PbS/CdS Janus-like Heterostructure Nanocrystals", *ACS Nano*, 12, 10, 10084-10094, **2018,** doi:10.1021/acsnano.8b04850

4. R.W. Crisp, G.F. Pach, J.M. Kurley, R.M. France, M. Reese, S.U. Nanayakkara, B.A. Macleod, D.V. Talapin, M.C. Beard, J.M. Luther, "Tandem solar cells from solution-processed CdTe and PbS quantum dots using a ZnTe:Cu/ZnO tunnel junction", 17(2), 1020-1027, *Nano Letters*, **2017**, doi:10.1021/acs.nanolett.6b04423

5. L. Kubie, M.S. Martinez, E. M. Miller, L. Wheeler, M.C. Beard, "Atomically thin metal sulfides", *JACS*, 141, 30, 12121-12127, **2019,** doi: 10.1021/jacs.9b05807

Summary Conclusions:

In this project we explored the use of semiconductor nanocrystals as a high efficiency solution deposited solar cell material. We considered two cases where semiconductor nanocrystals can enhance the solar cell power conversion efficiency. We considered MEG in PbSe QDs, heterostructured PbS/CdS nanostructures, low bandgap ternary QDs and tandem devices made from solution deposited nanocrystals. We developed a new synthesis of AMTS that have the potential to enhance the MEG efficiency. We demonstrated that solar cells can be fabricated from these nanocrystal systems.

Subject Inventions Listing:

U.S. Provisional Patent Application 62/697,739 (EXPIRED) – filed July 13, 2018; docket No. NREL 18-97.

ROI #:

ROI No. 18-97